CCFE
CULHAM CENTRE FOR FUSION ENERGY

UK Atomic Energy Authority

UKAEA-CCFE-PR(24)03

F.Eriksson, E.Tholerus, G.Corrigan, Y.Baranov,
X.Bonnin, D.Farina, L.Figini, L.Garzotti, S.H.Kim,
F.Koechl, A.Loarte, E.Militello Asp, C.Olde, V.Parail,
S.D.Pinches, A.Polevoi, P.Strand

Simulations of the stationary Q=10 and the exit phase from the flat-top of an ITER 15MA baseline scenario

Simulations of the stationary Q=10 and the exit phase from the flat-top of an ITER 15MA baseline scenario

F.Eriksson, E.Tholerus, G.Corrigan, Y.Baranov, X.Bonnin,
D.Farina, L.Figini, L.Garzotti, S.H.Kim, F.Koechl, A.Loarte,
E.Militello Asp, C.Olde, V.Parail, S.D.Pinches, A.Polevoi, P.Strand

This is a preprint of a paper submitted for publication in
Nuclear Fusion

Simulations of the exit phase from the flat-top of an ITER 15MA baseline scenario

Fully predictive JINTRAC simulations with consistent treatment of D and T in the whole plasma

F. Eriksson[1], E. Tholerus[1], G. Corrigan[1], Y. Baranov[1], X. Bonnin[2], D. Farina[3] , L. Figini[3], L. Garzotti[1], S.H. Kim[2], F. Koechl[1,2], A. Loarte[2], E. Militello Asp[1], C. Olde[1], V. Parail[1], S.D. Pinches[2], A. Polevoi[2] and P. Strand[4]

[1]UKAEA, Abingdon, United Kingdom
[2]ITER Organization, St. Paul Lez Duranze Cedex, France
[3]Instituto per la Scienza e la Tecnologia dei Plasmi, Milan, Italy
[4]Association EURATOM-VR Chalmers University of Technology, Göteborg, Sweden

Abstract. To design a safe termination scenario for a burning ITER plasma is a challenge that requires extensive core plasma and divertor modelling. The presented work consists of coupled core/edge/SOL/divertor simulations, performed with the JINTRAC code, studying the Q=10 flat-top phase and exit phase of the ITER 15MA/5.3T DT scenario. The modelling utilizes the recently implemented option to treat deuterium and tritium separately in the SOL/divertor enabling a consistent treatment of deuterium and tritium in the whole plasma volume which is a unique capability of JINTRAC. In addition, these are the first JINTRAC simulations of this scenario to use a first-principle transport model, self consistently model the ECRH power deposition and to include tungsten, keeping track of tungsten sputtering and accumulation. The flat-top simulations demonstrate the possibility of sustaining a steady state fusion Q of 10 using pure deuterium gas puff together with DT mixed pellets which is preferential as it allows a more effective use of tritium. Simulations of the exit phase is set up sequentially starting with a density decay at full current and auxiliary power that demonstrate the possibility to reduce the density safely within a few seconds. Following the density decay, a subsequent auxiliary power ramp down in H-mode is performed with a late H-L transition at low auxiliary power which is preferred for radial stability control. The final ramp-down phase consists of a current ramp-down in L-mode to 3.75MA.

1. Introduction

Integrated modelling is an important tool to self-consistently study the complex set of interactions occurring during all phases of the plasma discharge. To sustain optimal performance during the flat-top phase of the discharge as well as to safely exit from burning conditions, effects such as heating, fuelling, impurity radiation and accumulation are essential. The plasma also needs to stay within operational limits including limiting

heat loads on divertor targets and minimizing neutral beam shine through. The simulations in this paper are performed with the integrated modelling tool JINTRAC [1], unique in its capability to self-consistently model the core/edge and scrape-off-layer (SOL)/private region (PR) in a single framework. The scenario studied is the ITER 15MA/5.3T DT scenario including the flat-top, fusion Q=10 phase in H-mode and the subsequent termination of the discharge. The aim for the flat-top is to demonstrate the sustainment of a fusion Q of 10 using pure deuterium gas puff together with DT mixed pellets resulting in a deuterium rich plasma edge and close to a 50/50 mix of deuterium and tritium in the core for optimum fusion performance. The exit phase consists of the ramp-down of density at full auxiliary power and current followed by an auxiliary power ramp-down, an H-L transition, and finally, a current ramp-down in L-mode to 3MA. This ramp-down scenario differs from most previous simulations such as [2, 3] where the density is assumed to linearly drop with the current. With the inclusion of the particle transport and a consistent treatment of core/edge/SOL/PR interactions these simulations have the capability to study how fast the density decreases when the pellet fuelling is changed. Knowing the characteristic time of density decay for a given ITER fuelling system while maintaining H-mode and divertor heat load and density control will be important for safe emergency termination scenarios and designing ramp-down simulations with magnetic control including shape control, vertical stabilization, and force limits on the coils systems. The result of the density decay rate study can also be used to set the rate for a simultaneous density, current decay scenario. Compared to previous JINTRAC simulations of this scenario, presented in [2, 3] several improvements have been made to the modelling set-up including the additions of the EC code GRAY [4] to simulate the EC deposition and current drive self-consistently, the first-principle transport model EDWM [5] for anomalous core transport, the inclusion of tungsten in the plasma and, deuterium and tritium are now for the first time treated separately in the whole plasma volume [6]. The divertor heat load has been re-modelled to include contributions not only from the ion-, and electron particle fluxes, heat fluxes and recombination processes‡, but now, at runtime, with additional contributions from neutral heat loading, reflected heat and, kinetic energy, enabling improved monitoring and control. The scenario envisaged here relies on the divertor staying in a partially detached state for density control purposes, meaning a total divertor heat load below $10MW/m^2$ and strike point electron and ion temperature above 1eV. Accurate calculation and runtime control is therefore one essential aspect of this work.

The rest of the paper is organized as follows: In Section 2 more details of the modelling setup is presented. Section 3 consist of results of the simulations of the flat-top and 4 the subsequent exit of the plasma from burning conditions. Finally, summary and conclusions are given in Section 5.

‡ which has been used previously in post-processing

2. Modelling setup

The modelling in this work is performed with the JINTRAC code, which combines the 1.5D core transport solver JETTO [7] and the 2D transport solver EDGE2D [8] for the SOL/PR. JETTO itself is coupled to other models to include effects such as heating and particle sources from auxiliary heating and pellet fuelling, ohmic heating and fusion reactions, current drive and diffusion, impurities, equilibrium calculation and MHD instabilities. EDGE2D is coupled to EIRENE [9] to enable modelling of the plasma and neutrals in the SOL/PR including gas puff and pumping, sputtering and recycling from the tungsten divertor and beryllium first wall. The simulations presented in this paper utilize the recently implemented option of treating deuterium and tritium separately in EDGE2D resulting in a fully consistent treatment of deuterium and tritium in the whole plasma volume. For computational reasons, a partial coupling scheme is used allowing JETTO to advance for a maximum of 3ms without advancing EDGE2D followed by a 1ms coupled phase. A correction is used to compensate for the non-conservation of particle flux during the uncoupled phase by temporarily changing the particle source and approximate a fully coupled run. Note that running JETTO coupled to EDGE2D/EIRENE necessitates a fixed plasma boundary which means that effects from an evolving plasma volume during the exit phase of the discharge is not included in these simulations.

The fuelling for the $Q = 10$ ITER baseline scenario is expected to need a combination of gas puff and pellets [10] due to large plasma volume and high edge densities and temperatures making gas fuelling alone insufficient. In this paper the fuelling scheme consists of pure deuterium gas puff together with DT mixed pellets. The pellets are launched from the high field side upper launcher, see Fig. 1, with velocity $300m/s$ which is the expected maximum intact pellet speed for ITER [11]. Sizes used are 0.2cm radius spherical pellets in the high-density flat-top phase and a reduced 0.14cm radius in the low-density phase of the simulations, to reduce the density fluctuations during the pellet cycle, with a composition of 45/55 mixed DT in H-mode and pure D in L-mode. The larger pellet size is in the lower range of expected pellet volumes for the ITER pellet injection system [10]. The pellet frequency is adapted by a feedback scheme to keep a specified Greenwald density fraction ($< n_e > /n_{GW}$ where $< n_e >$ is the line averaged electron density and $n_{GW} = I/\pi a^2$ is the Greenwald density), the evolution of which is shown in Fig. 2. To model the pellet ablation and particle deposition the HPI2 code [12] is used. The maximum change in electron density during a pellet cycle in flat-top, shown in Fig. 3, illustrates a pellet deposition with a peak at $\rho_t = 0.85$ (defined as the square root of normalized toroidal flux) consistent with previous pellet modelling for this scenario cf. [13]. In addition to pellets, the plasma is fuelled with deuterium gas, puffed from the upper SOL, at a rate between $0.5{*}10^{22}/s$ and $3{*}10^{22}/s$. In the end of the final phase of the current ramp-down, when the total current has reached 10MA, pure deuterium gas puff is used to fuel the plasma. The gas puff rate is then under feedback control keeping 20% Greenwald density fraction for the remainder of the simulation (which can be seen in Fig. 2). A higher rate helps to cool down the divertor target plates limiting

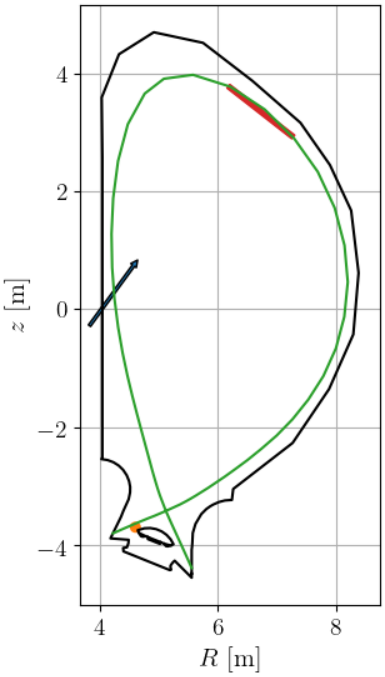

Figure 1. 2D illustration of the ITER wall, plasma separatrix (green), D gas puff location in the upper SOL (red), Ne seeding in the private region (orange dot) and high field side upper pellet injector (black arrow) used in the simulation.

the heat load to targets though the main technique used to avoid prolonged maximum heat loads above the maximum limit of $10MW/m^2$ is neon seeding. Neon is injected from an inlet valve in the private region, also shown in Fig. 1, under feedback control on the maximum heat load to target. Neon seeding with a maximum rate of $2.5 * 10^{20}/s$ is activated when the maximum heat load exceeds $8MW/m^2$ which subsequently radiates and cools down the target plates reducing the heat load. The neon seeding is set up like this in order to limit the risk of excessive radiation of neon in the SOL that can lead to full detachment of the plasma. A semi-detached plasma is important for density control in ITER. In addition, for numerical reasons, important molecular reactions needed to properly simulate detachment are not included in the neutrals model used within EIRENE in these simulations and therefore the plasma needs to remain partially detached. Like previous ITER modelling with JINTRAC [3], a reduced NIMBUS-like neutral model is used instead of the full EIRENE neutral model (Kotov2008 [14] without neutral-neutral collisions and opacity) allowing the use of a source linearisation scheme within EDGE2D that speeds up the simulation and makes them more numerically robust. (Details in Appendix B of [3]). In addition to neon, impurities included are helium and tungsten with reaction cross sections determined by the ADAS database. Zero redeposition of sputtered tungsten is used to study the worst possible case.

The heating scheme used consists of the originally designed heating scheme [15] of 33MW

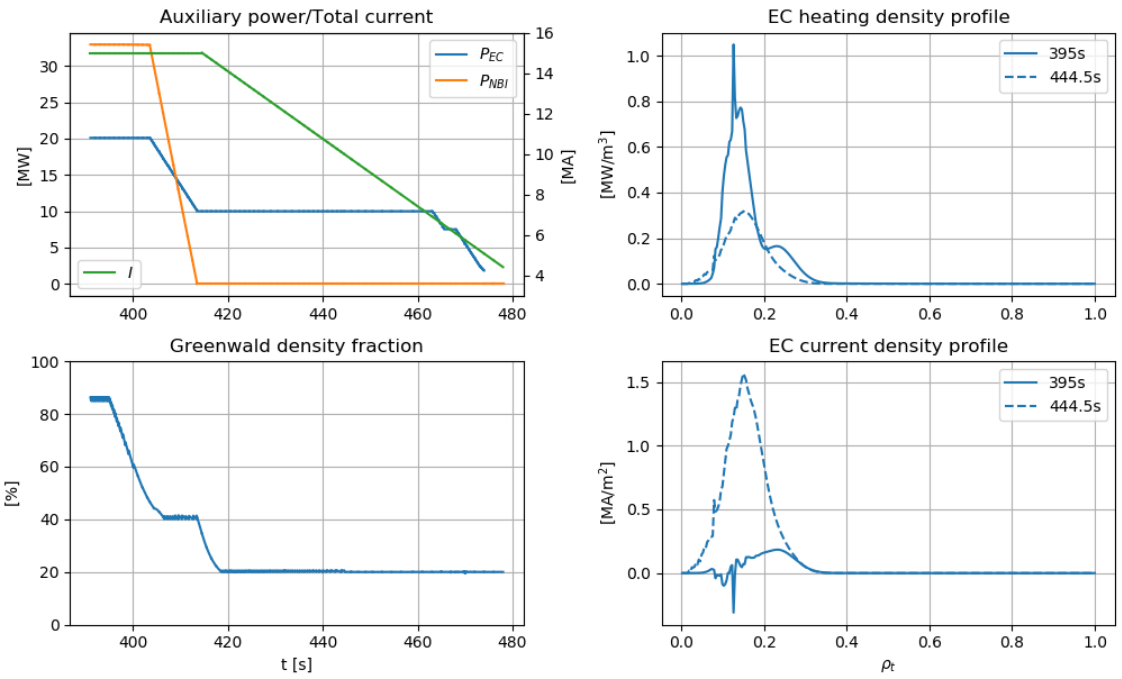

Figure 2. Evolution of the auxiliary power and total current (upper left) and Greenwald density fraction (lower left) during the flat top and all stages of the exit phase. EC heating and current deposition at the end of the flat top phase (upper right) and when total current is down to 10MA in L-mode (lower right).

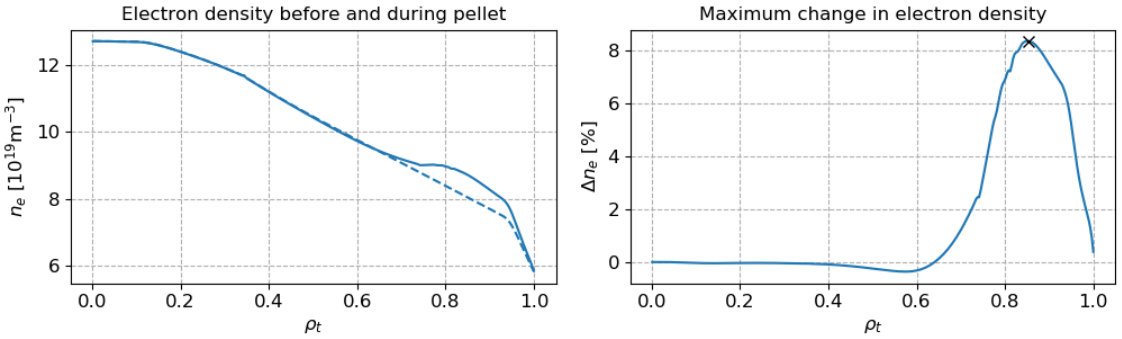

Figure 3. Electron density just before and after a pellet during flat-top (left) and maximum percentage of change in the electron density during the pellet cycle (right). The cross at $\rho_t = 0.85$ represent the peak of the pellet deposition.

NBI (pure D beams) and 20MW EC in the flat-top phase of the simulation which is gradually reduced during the exit phase. To have a fast and reliable calculation of the heat and particle deposition profiles from the neutral beams the PENCIL code [16] is used. For self-consistent modelling of the EC power deposition and current drive the beam-tracing code GRAY is used. The 20MW EC power is divided equally between the top, mid and bottom equatorial launcher in O-mode using 170GHz. The poloidal angles are set to optimize the electron heating in the region of $\rho_t = 0.1 - 0.3$, to avoid tungsten accumulation, while minimizing

the negative driven current from the top equatorial launcher. The resulting heat and current deposition profiles at full power in the flat-top and during the final phase of the ramp down when total current is down to 10MA are shown in Fig. 2 together with the evolution of the auxiliary power and current during the exit phase. A gradual reduction of the auxiliary power is made during the exit phase for two main reasons. First, a gradual reduction of the auxiliary power and consequently also the fusion power has been shown to limit the drop in poloidal beta which is beneficial for vertical stability control reducing the risk of disruption [**?**]. Secondly, a slower variation of the plasma stored energy helps avoid tungsten accumulation and excessive heat loads during the exit phase [17]. The NBI power is here linearly reduced to zero over 10s and, over the same time scale, the EC power is reduced with 10MW EC power kept between the mid and bottom equatorial launchers to help avoid full detachment [2]. A final reduction of the EC power down to zero is made when the total current is 7MA.

For the H to L transition, the L to H power threshold, P_{L-H}, is set according to the Martin scaling [18]

$$P_{L-H} = 0.0488 < n_{e,20} >^{0.717} B_{tor}^{0.803} S^{0.941} \frac{2}{A_{eff}} \tag{1}$$

in (MW), where $< n_{e,20} >$ is the line averaged electron density in $10^{20}/m^3$, B_{tor} is the toroidal magnetic field on axis in T and S is the plasma surface area in m^2 and

$$A_{eff} = \frac{2 < n_D > +3 < n_T >}{< n_D > + < n_T >} \tag{2}$$

is the effective isotope mass in a DT plasma. Note that the inclusion of a mass scaling results in a 20% reduction for DT plasmas compared to a pure D plasmas. For ITER, the Martin scaling law is expected to be valid above the density corresponding to a Greenwald density fraction $f_{GW} =< n_e > /n_{GW} = 40\%$ [15]. The power threshold is compared against

$$P_{comp} = P_{aux} + P_{\alpha} + P_{ohm} - P_{rad} - < \frac{dW_P}{dt} >, \tag{3}$$

where $< dW_P/dt >$ is the time derivative of the stored plasma energy time averaged over 5ms to reduce the noise in dW_P/dt. An H to L transition is triggered when $P_{comp} < P_{L-H}$. To avoid an instantaneous change between suppression and non-suppression of the transport within the pedestal region in H- and L-mode respectively a gradual change from suppression to non-suppression is set by multiplying the anomalous transport within the suppressed region by a factor

$$e^{-(P_{comp}-P_{L-H})/P_{L-H}/0.05} \tag{4}$$

when $(P_{comp} - P_{L-H})/P_{L-H} > 0$.

Once in L-mode, the total current, which is 15MA in flat-top, is linearly reduced at a rate of 5MA over 30s ($\sim$0.17MA/s), to stay within the range of controlled plasma current ramp-down [19], to 10MA during the exit phase. A total current boundary condition is used for the predictive current profile calculation where the total current satisfies the current diffusion

equation with contributions from an inductive current from the central solenoid together with contributions from the non-inductive current from auxiliary heating, a bootstrap current and an ohmic current. The magnetic equilibrium is calculated every 100ms with the equilibrium solver ESCO inside a prescribed, fixed last closed flux surface boundary. For the region inside the outer radii where the safety factor crosses the q=1 surface, a continuous sawtooth model is used to include a time averaged effect of sawteeth. The presence of ELM control schemes is assumed so the effect of ELMs is chosen to be time averaged by using a continuous ELM model. The pedestal width and maximum achievable pedestal pressure are imposed limiting the edge pressure gradients to a specified α_{crit} set to 1.9 [20]. The effect of discrete ELMs on the Q=10 flat-top phase of this scenario has been shown to result in increase in tungsten levels in the core and SOL/PR [21].

For the transport in the plasma core, the neoclassical transport is modelled by NCLASS [22] and the anomalous transport is modelled with EDWM. A 10% Bohm coefficient is added in H-mode for numerical stability and, to model the increase in transport in L-mode, the Bohm/gyro-Bohm L-mode model is used together with the EDWM model. In addition to the improvement in its predictive capability compared to previously used Bohm/gyro-Bohm model, the choice of EDWM is motivated by its resilience simulating inverted profiles occurring in ITER edge fuelling dominated plasma and its computational speed.

In the SOL, perpendicular heat and particle transport is described with radially dependent transport coefficients. The near SOL is matched to the values at the separatrix with a gradual transition to prescribed values in the far SOL. When the value at the separatrix exceeds the prescribed value in the far SOL value (i.e. L-mode or during ELM) an exponential decay is used. Inter ELM (or with continuous) ELM, when the value at the separatrix is less than prescribed in the far SOL a barrier extends into the SOL which then rises with a tanh dependency to the far SOL value. More details and sensitivity studies to SOL transport coefficients are available in [23, 24]. Below the x-point the perpendicular transport is set constant. Parallel transport in the SOL is calculated from a 21 moment description with a closure taking into account non-trace multi-species levels which is necessary to be able to treat D and T separately [25]. Cross-field drifts are not included.

3. Flat-top with Fusion Q=10

The flat-top phase of the simulations start at 391s before which the simulations were running with the described setup in Sec. 2...

initial condition

How to formulate that our initial conditions consist of a Q=10 plasma with the described setup that has been running while we are gradually fixing bugs in segregated DT in EDGE2D??

The flat-top phase of the simulation is set up with a Greenwald density fraction of

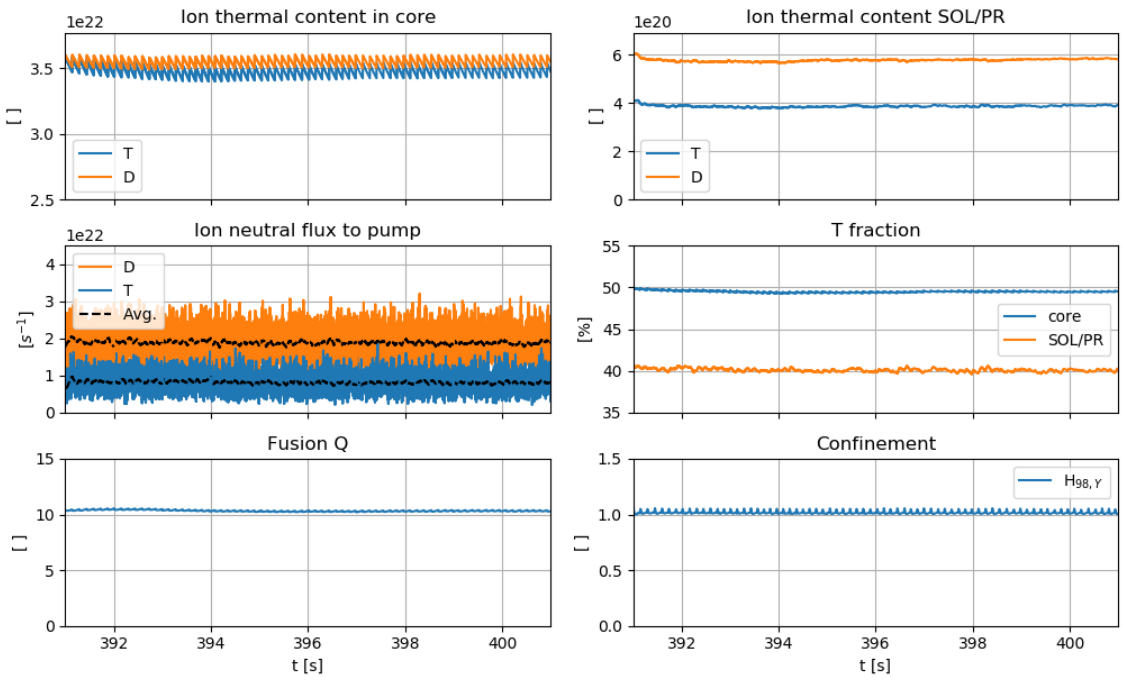

Figure 4. Time traces illustrating the steady state phase of the simulation for 45/55 DT mixed pellets and pure D gas puff. The average flux to pump for D and T is time averaged over 0.1s.

85% resulting in a pellet frequency of 8Hz using the chosen fuelling scheme. As illustrated in Fig. 4, the ion content in the core and edge are kept steady when the pellet is slightly tritium rich together with the pure deuterium gas puff. The resulting total fuelling rate of $2 * 10^{22}/s$ for D and $0.9 * 10^{22}/s$ for T is well within operational limits for both the total and the tritium throughput in the ITER design [26]. Also, the combined total fuelling rate is consistent with previous JINTRAC simulations of this scenario [2] and the individual deuterium and tritium rates balances well the average flux to the pump in Fig. 4. The tritium fraction is 49.5% in the core and 40% in the SOL/PR due to the asymmetry of the fuelling scheme between D and T. Even with this asymmetry, the simulations show that it is possible to sustain a fusion Q of 10. The final time trace in Fig. 4 consists of the confinement factor H_{ITP98} (radiation corrected) which is 1 throughout the flat-top simulations showing that the calculated transport is consistent with the ITER scaling law [27].

As shown in Fig. 5, the maximum heat load is kept just below the limit of $10MW/m^2$ throughout the flat-top phase of the simulation using neon seeding. The neon content is subsequently tied to the heat load on the divertor targets. After 4s the level of neon saturates at 0.3% and the average neon pumped out is equal to the average of the injected and recycled neon resulting in a radiation level of 7MW in the core during steady state. Total core radiation including bremsstrahlung and synchrotron radiation is 25MW consistent to previous JINTRAC simulations of this scenario [2]. This reasonable amount of neon will be important during the low-density, current ramp-down phase to avoid excessive cooling

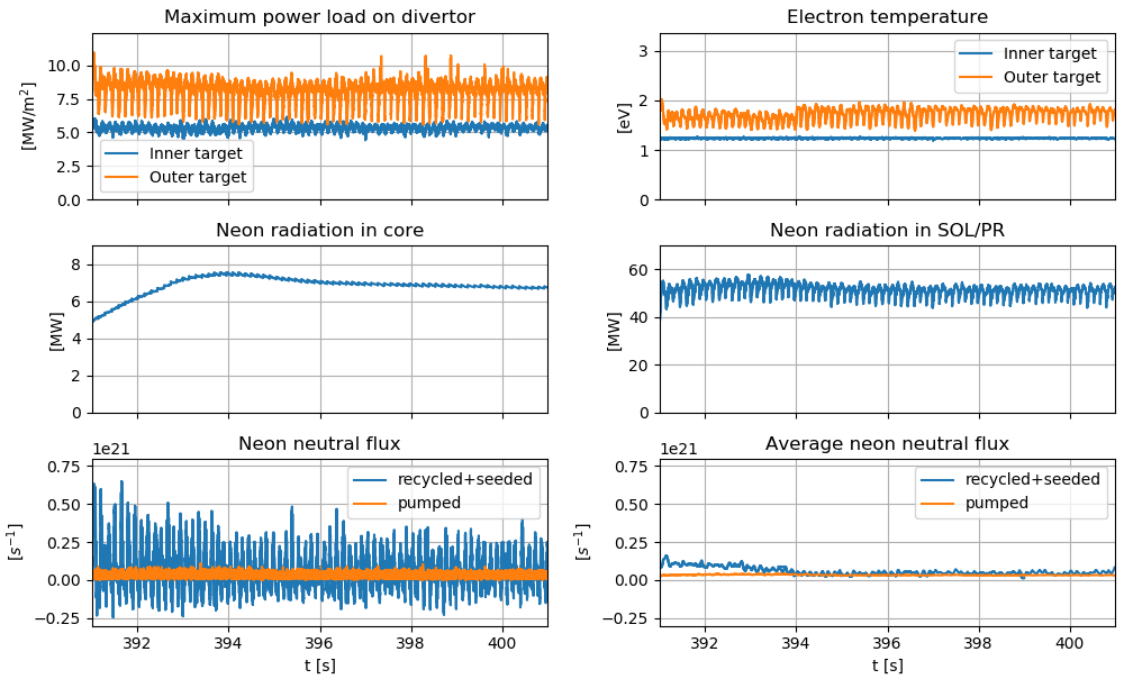

Figure 5. Time traces illustrating the steady state phase of the simulation for a 45/55 DT pellet and pure D gas puff. The maximum heat load to target as well as the neon radiation in core and SOL/PR. The neon neutral flux is time averaged over 0.05s in the bottom right figure.

of the divertor targets which can result in full detachment. Also in Fig. 5 is the electron temperature at the inner and outer strike point of the divertor targets. Both of which remain steady and above the 1eV limit for avoiding detachment. In addition, the divertor region where recombination rate is higher than the ionisation rate is limited to the private region below the target plates as illustrated in 6. In a fully detached plasma this region would spread above the target plates.

The final time trace demonstrating the steady state for this scenario is presented in Fig. 7 with a source rate from fusion reactions of $2 * 10^{20}/s$ which matches the time averaged helium pump rate. The helium level in the core saturates at 1.9% which is slightly lower than previous simulation of this scenario [2]. Finally, the results of Fig. 7 demonstrate that in addition to maintaining acceptable divertor heat loads with low levels of neon at fusion Q of 10, the tungsten sputtering and resulting tungsten radiation remain very low and there is no accumulation in the core even without any redeposition of tungsten. Worth noting is that when discrete ELMs are used, the sputtering levels are significantly increased [21]. Also, compared to JINTRAC simulations where D and T are combined into a single species in EDGE2D a factor on the order of two difference in sputtering yield comes from the normalisation changing from DT density combined to T density.

Profiles in the flat-top phase (at 395s) for deuterium, tritium, helium, neon and tungsten are presented in Fig. 8. The density peaking is marginally higher for tritium than deuterium

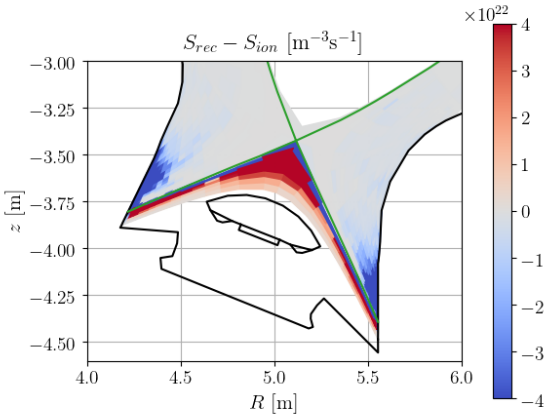

Figure 6. 2D plot of ionisation/recombination balance at 395s including the separatrix in green and the wall in black.

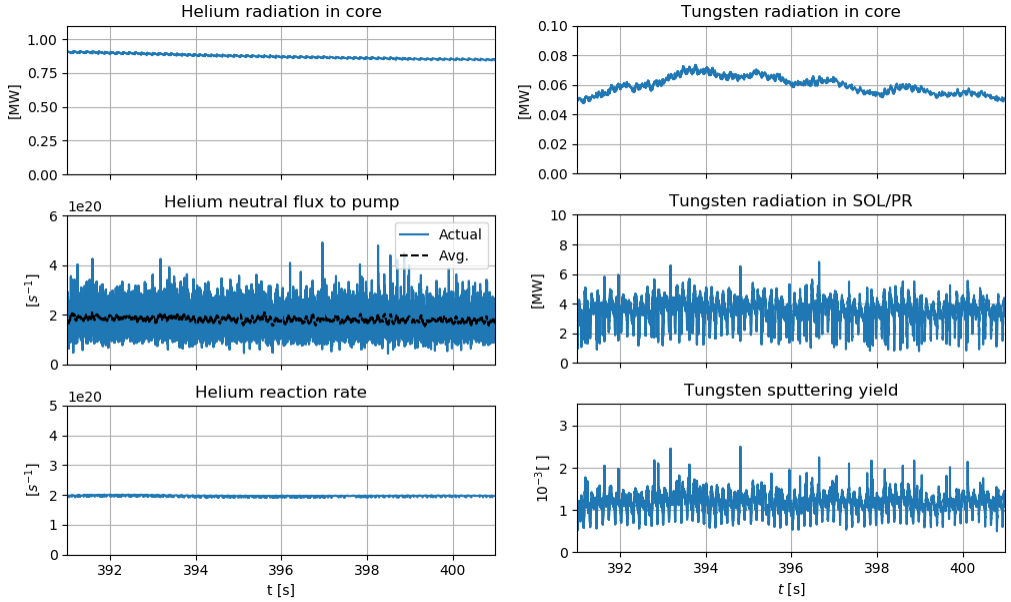

Figure 7. Time traces illustrating the steady state phase of the simulation for a 45/55 DT pellet and pure D gas puff. The helium flux to the pump is time averaged over 0.05s in middle left plot. Tungsten sputtering yield is normalized to a main ion species which is tritium for these simulations.

in part due to the 45/55 DT mix in the pellets which penetrates further into the core than the deuterium gas puff and in part due to difference in transport between D and T. The pure deuterium gas puff also results in a deuterium rich edge. Ion temperature is 14.8keV on axis resulting in a fusion Q of 10.3 for the duration of the flat-top phase. Also in Fig. 8 is the contributions to the heating and current density with resulting safety factor. As expected, the dominant contribution to the heating power is from the alpha heating and the total current is dominated by the inductive current with a small contribution from the auxiliary

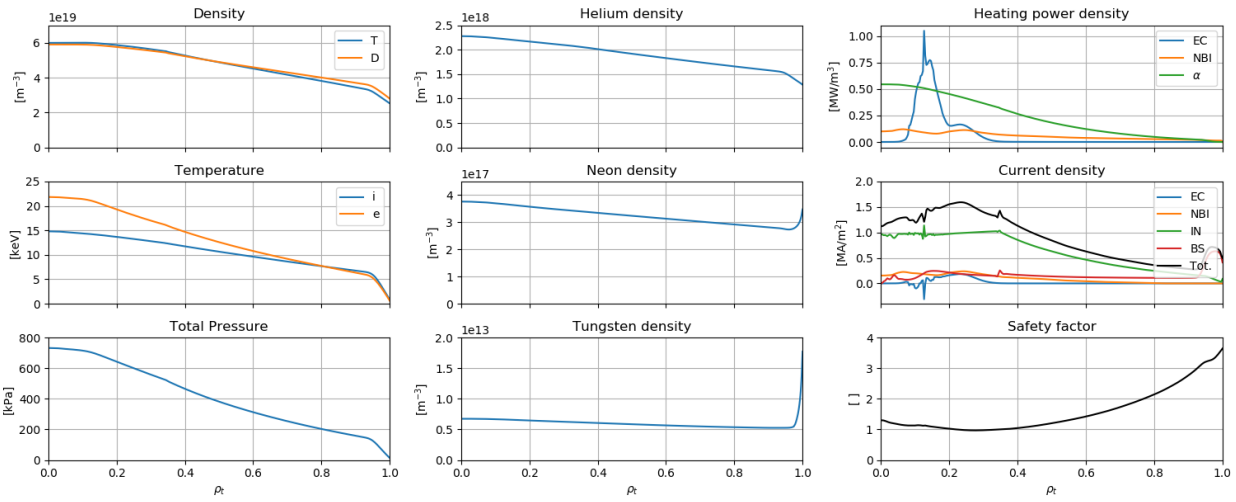

Figure 8. Core profiles at 395s, in the flat-top phase.

power and bootstrap current. The safety factor crosses the q=1 surface twice with the outer most point around $\rho_t = 0.3$. Inside this region the continuous sawtooth model is active. Worth noting is that given the current diffusion time scale the current density shape and corresponding q-profile, particularly on axis where the resistivity is lowest, will be influenced by the initial condition of previous JINTRAC simulations [3] upon which these simulations originate.

A 2D plot of the deuterium density and the ratio of tritium to deuterium density is shown in Fig.9. We observe that deuterium is dominant in the far SOL as well as in the private region below the target plate. To clarify the difference between deuterium and tritium in the SOL, the density profile along the outer midplane is shown in Fig.10.

4. Exit phase

At the time of starting the simulations of the exit phase, the flat-top consisted of the initial 4s of simulations. Therefore, the exit phase starts at 395s with the sequential ramp down of density, power and current.

4.1. Density decay at full auxiliary power and current

Starting from flat-top Q=10 burning conditions the exit phase is initialised with a density decay at full auxiliary power and current, keeping the plasma in H-mode. During this phase the density is reduced from the flat-top density at Greenwald density fraction 85% down to 45% which reduces the fusion Q to ~ 5. For the density decay phase two cases are considered with summary time traces depicted in Fig. 11. In the first case the pellets are instantaneously switched off and in the second a linear reduction of 5% per second of the Greenwald density fraction is specified which corresponds to an almost linear reduction of the pellet frequency

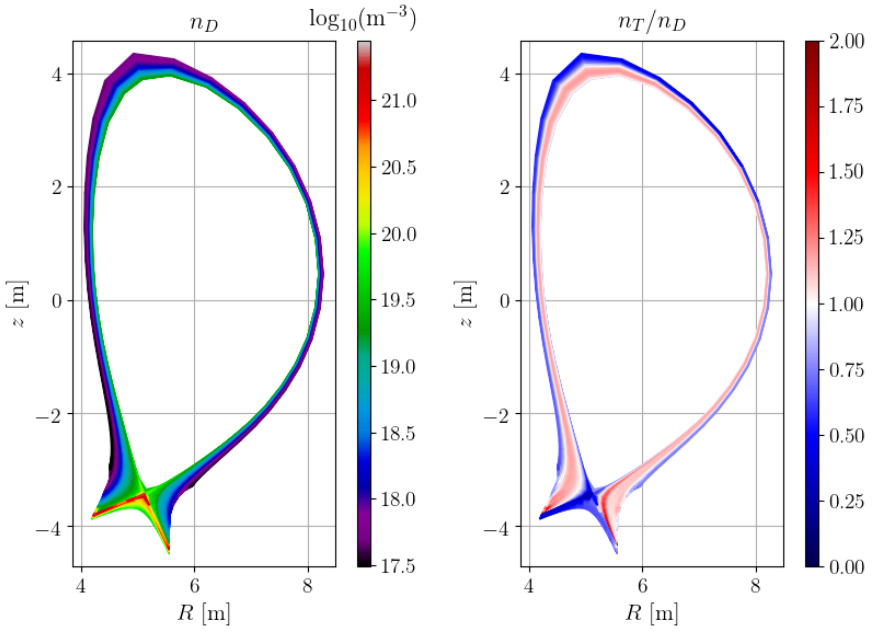

Figure 9. 2D profiles of the deuterium ion density and the ratio of tritium to deuterium density in the SOL/PR at 395s, in the flat-top phase.

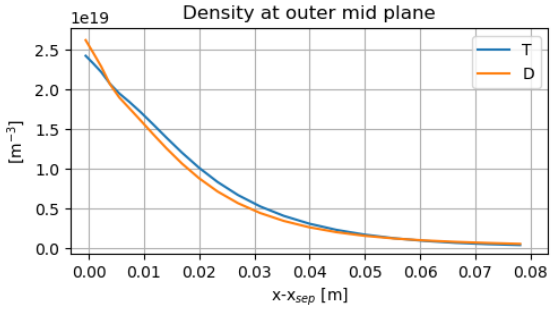

Figure 10. Deuterium and tritium density profiles along the outer mid plane at 395s. The radial grid extends slightly inside the separatrix.

from 8Hz to 0Hz over 5s. As the density reduces there is an initial increase in fusion Q, due to increase of the ion temperature, and a momentary increase in the heat load to target. This triggers the neon seeding and there is a subsequent increase in neon in the edge and core. With the continued reduction of density, the ion temperature reduces, and the heat load is once again below the limit triggering the neon seeding and the neon content is then steadily pumped out reducing the content in the core and edge. There is also an increase in tungsten sputtering and the tungsten content in the core increases though from very low levels. When the density decays over the slightly longer timescale in the second case, the maximum heat load is kept under the limit of $10MW/m^2$, except short spikes coinciding with the pellets. As the density is reduced at full NBI power, the NBI shine-through is

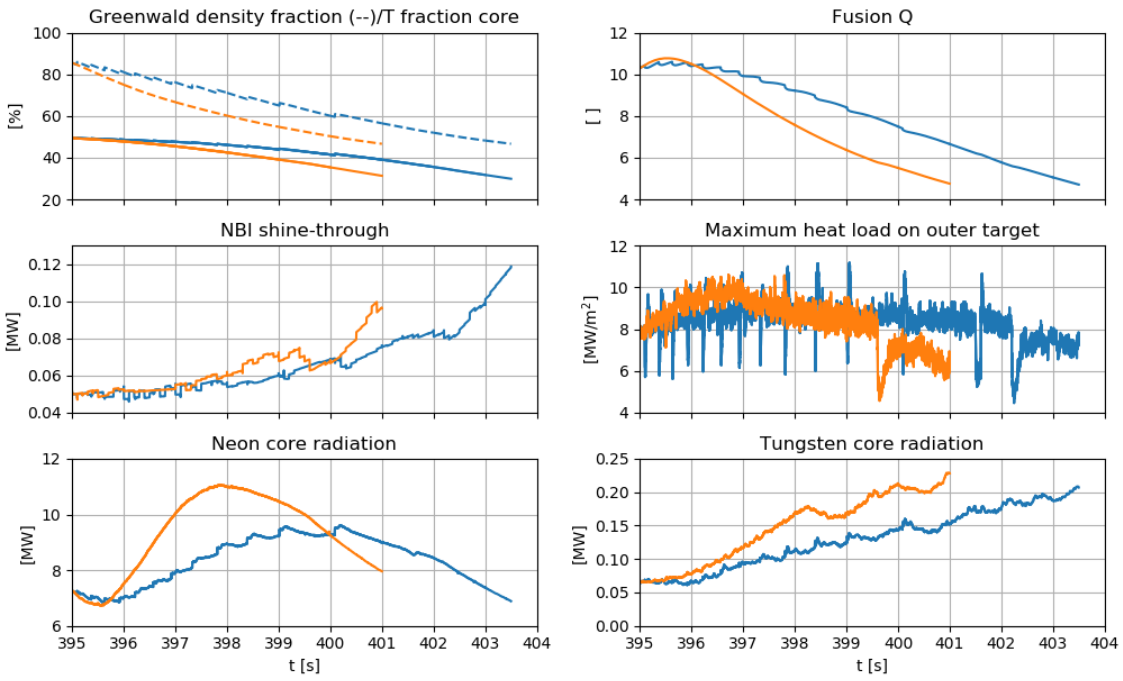

Figure 11. Time evolution during the density decay phase at full auxiliary power and current. Linear reduction of $5\%/s$ of Greenwald density fraction (blue) and pellet switch off (orange).

increasing from levels of 0.05MW at flat-top to 0.1MW and 0.12MW for the first and second case respectively, which is well within acceptable levels. Worth noting, as seen in Fig. 11 the trends are very similar in the two cases and none of them result in any lasting issues in terms of radiation from tungsten in the core, excessive cool down of the target risking full detachment or long exposure to too high heat loads. To limit the increase in heat load to target during the initial density decay at high fusion Q the remaining of the exit phase is continued from the end of the slower density decay phase.

2s into the slower density decay phase, which is the point of highest maximum heat load to target in this case, the heat load distribution as well as the temperatures along the target plates are shown in Fig. 12. At the radial point of maximum heat load the electron and ion temperature are equal at 3.2eV and 1.4eV at the inner target and outer target respectively. This is below the 5eV level estimate for issues with excessive tungsten sputtering. Also shown in Fig. 12 is the 2D profile of the total impurity radiation in the SOL/divertor region at this time which is dominated by the neon radiation in the divertor region. As mentioned above, this amount of neon causes no issues related to detachment and will gradually reduce during the remaining exit phase.

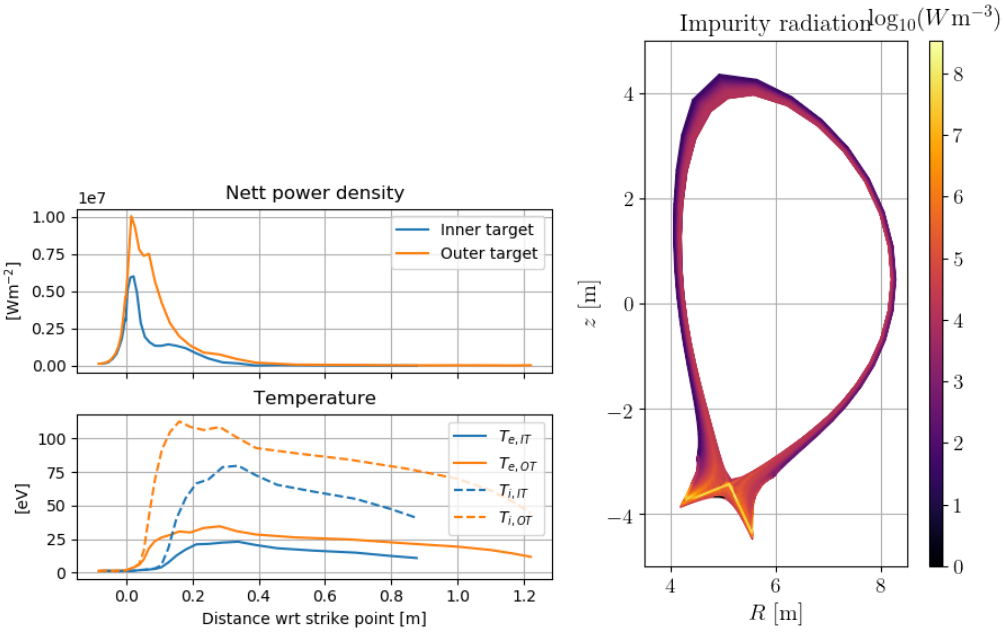

Figure 12. Power density and temperature profiles along the inner and outer target at 397s, 2s into the density decay at full current and auxiliary power (left) when the heat load to the target is the highest during the density decay. 2D profiles of the total impurity radiation in the SOL/divertor region (right) at this time. ADD SUBPLOT OF TI AND TE ZOOMED IN AROUND PEAK HEAT LOAD LOCATION?

4.2. Auxiliary power ramp down at full current and H to L transition

Following the 8s density decay, corresponding to the longer of the two studied cases in Sec. 4.1, is an auxiliary power ramp-down. As described in Sec. 2 and illustrated in Fig. 13, the auxiliary power is reduced linearly over 10s starting at 403.5s. Pellet fuelling is used to keep the Greenwald density fraction at 40% to maintain the validity of the Martin scaling for the H-L power threshold and to limit the reduction in fusion power. With the reduction of the pellet frequency during the previous density decay, the tritium content in the core reduced at a higher rate than the deuterium which slowed down due to the deuterium gas puff. The tritium fraction in the core, which was 50% during the flat-top was reduced to 30% by the start of the auxiliary power ramp-down and remain just below 20% when the pellets are again needed to keep the Greenwald density fraction from falling below 20%. At this density and tritium fraction the resulting H-L power threshold is around 49MW, shown in Fig. 13, and the remaining fusion power and auxiliary power are high enough to keep the plasma in H-mode throughout the auxiliary power descent as intended. 7s into the auxiliary power decrease, the edge ballooning parameter α falls below α_{crit} indicating a transition from type I ELMy regime to ELM free H-mode . 3s later, at the end of the the auxiliary power rampdown, when the NBI power is down to zero and the EC power is down to 10MW $P_{comp} \approx P_{L-H}$ and the H-L transition starts. At this time the plasma is dithering between

correct?

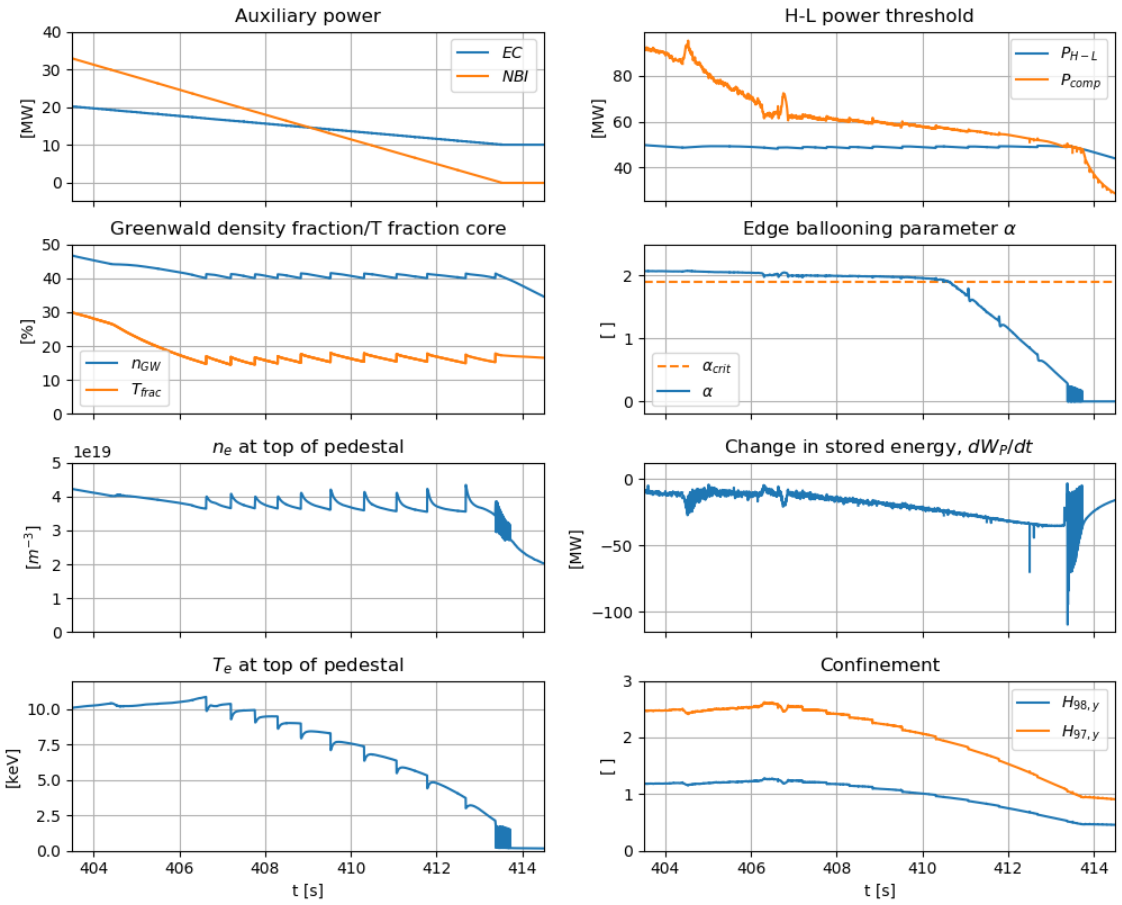

Figure 13. Time traces of the auxiliary power ramp-down starting at 403.5s and subsequent H-L transition ∼413.5s.

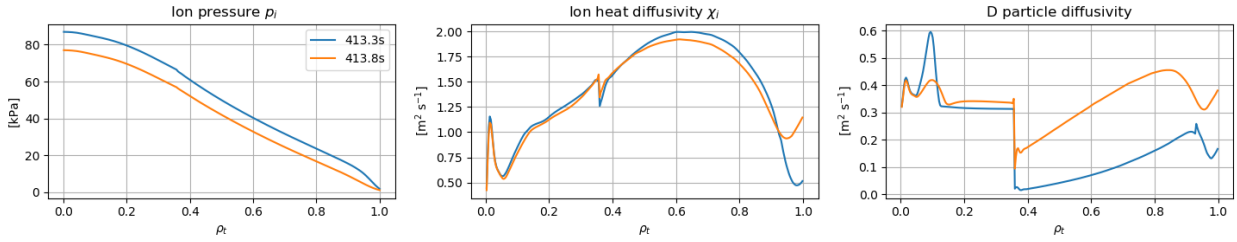

Figure 14. Profiles before and after the H-L transition.

H- and L-mode for $\sim 0.4s$ before it transitions to L-mode and remains there throughout the rest of the exit phase. Profiles of the ion pressure and the ion heat and particle diffusivity is shown in Fig. 14 before and after the H-L transition illustrating the effect of the increase in transport at the edge in L-mode. For the heat diffusivity the main difference between the H- and L-mode phase shown is from the change in Bohm transport while the deuterium particle diffusivity also has difference in anomalous transport from EDWM.

Fig. 15 illustrate the effect on the maximum heat load to target at different deuterium

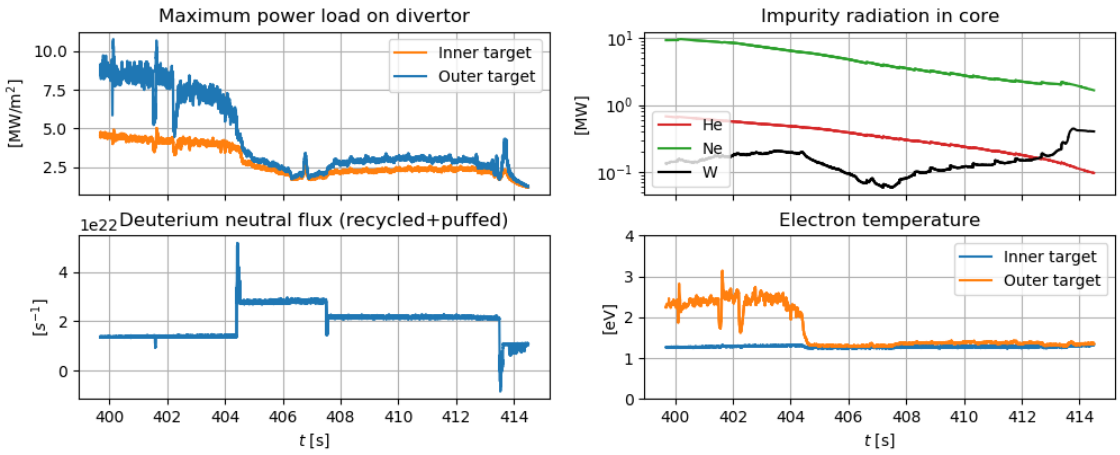

Figure 15. Time traces of the auxiliary power ramp-down starting at 403.5s and subsequent H-L transition ∼413.5s.

gas puff levels during the auxiliary power ramp-down. The time traces also include the last few seconds of the density decay at full power. As the density decreases at full auxiliary power the heat load to target gradually reduces and then there is a large drop in maximum heat load and electron temperature at the inner strike point coinciding with an increase in deuterium gas puff from $1.3 * 10^{22}/s$ to $3 * 10^{22}/s$. This reduced level of the maximum heat load to target $\sim 3MW/s^2$ at both inner and outer target reduce even further in the remaining L-mode phase (not in Fig. 15). There is a small increase in tungsten content during the H-L transition though no core accumulation occurs, and the neon is pumped out reducing the neon content throughout the remainder of the simulation.

4.3. Current ramp-down in L-mode

In the final step of the exit phase the total current is linearly reduced from 15MA to 3.75MA at a rate of ∼0.17MA/s at a fixed Greenwald density fraction and auxiliary power in L-mode. Following [2] and keeping some EC power throughout the majority of the ramp-down the issue with divertor detachment is avoided. As described in Sec. 2, pellet fuelling us used throughout all stages of the exit phase. When the total current is down to 10MA at 445s the pellet fuelling is turned off and deuterium gas puff alone is sufficient to keep the density at the specified Greenwald density fraction. At this point the tritium species, which is only trace at this point, is removed from EDGE2D for numerical reasons.

Selected time traces of entire exit phase, including the density decay, auxiliary power ramp-down and current ramp-down, are presented in Fig. 16. First of all, note that in flat-top the inductive current is about two thirds of the total current and the bootstrap current make up the majority of the remaining current. With the reduction of density at full auxiliary power the NBI driven current increases as the bootstrap current falls. By the time the plasma is in L-mode at low density, low auxiliary power the majority of the total current is inductive. The change in magnetic flux consumption needed is shown at the last closed

flux surface in Fig. 16 and the loop voltage is the total corresponding to that in the central solenoid in addition to the PF coils and the voltage induced by the plasma. The spikes in loop voltage coincide with the magnetic equilibrium updates in ESCO. Also worth noting is the build-up of a current hole on axis with the reduction of total current. The bootstrap current on axis is very low at these low densities and the inductive current is gradually reduced on axis. This loss of current on axis eventually leads to an exploding value of safety factor on axis and the numerical failure of the simulation. To limit the current hole on axis we use a model in JINTRAC to mimic the MHD instabilities occurring in current holes that result in a positive central current. The central resistivity is increased to the value at the outer edge of the current hole. The effect of which is clearly seen in the evolution of q_0 in Fig. 16. Finally, the plasma internal inductance increases steadily as the current is decreased. To ensure vertical stability in this phase vertical stability control including plasma shaping is used in the experiment. Since the plasma boundary is fixed in these simulations this is not included in the modelling presented in this work. The increase in internal inductance and reduction in poloidal beta both known to reduce vertical stability margin [28] show similar trends of previous ITER ramp-down simulations [29]. The vertical stability appears to be within the stability margin down to ∼7MA if we consider the indirect comparison with CORSICA [30] cases, shown in Fig. 17 and published in [29] and [31]. However, due to the fixed plasma shape assumed, an adequate evaluation of the stability or stability margin would be required a further work using more adequate modelling tool such as DINA or ITER HFPS which is under development.

Either add citation or remove "such as DINA or ITER HFPS which is under development"

5. Summary and conclusions

The presented work consists of the details of the sustainment of the flat-top Q=10 phase and the step-wise approach for the safe termination of plasma for ITER 15MA baseline scenario. The flat-top simulations demonstrate the possibility of sustaining a fusion Q of 10 using DT pellets and pure deuterium gas puff, which is preferential as it allows a more effective use of tritium, while staying within operational limits and keeping track of tungsten sputtering and accumulation as well as neon seeding. Using this fuelling scheme requires that the pellet mix is slightly tritium rich to keep 50/50 mix of deuterium and tritium in the core. The maximum heat load to target is kept just below the operational limit of $10 MW/m^2$ with neon seeding under feedback from the private region. The amount of neon is saturated during the flat-top phase at a level that does not cause any detachment during the exit phase and there is no tungsten accumulation occurring. The sequential setup for the exit phase consists of a gradual reduction of density at full auxiliary power and current followed by a ramp down of the auxiliary power, a late H-L transition and finally a current ramp down in L-mode. The density decay phase shows the promising result that the density can be reduced safely

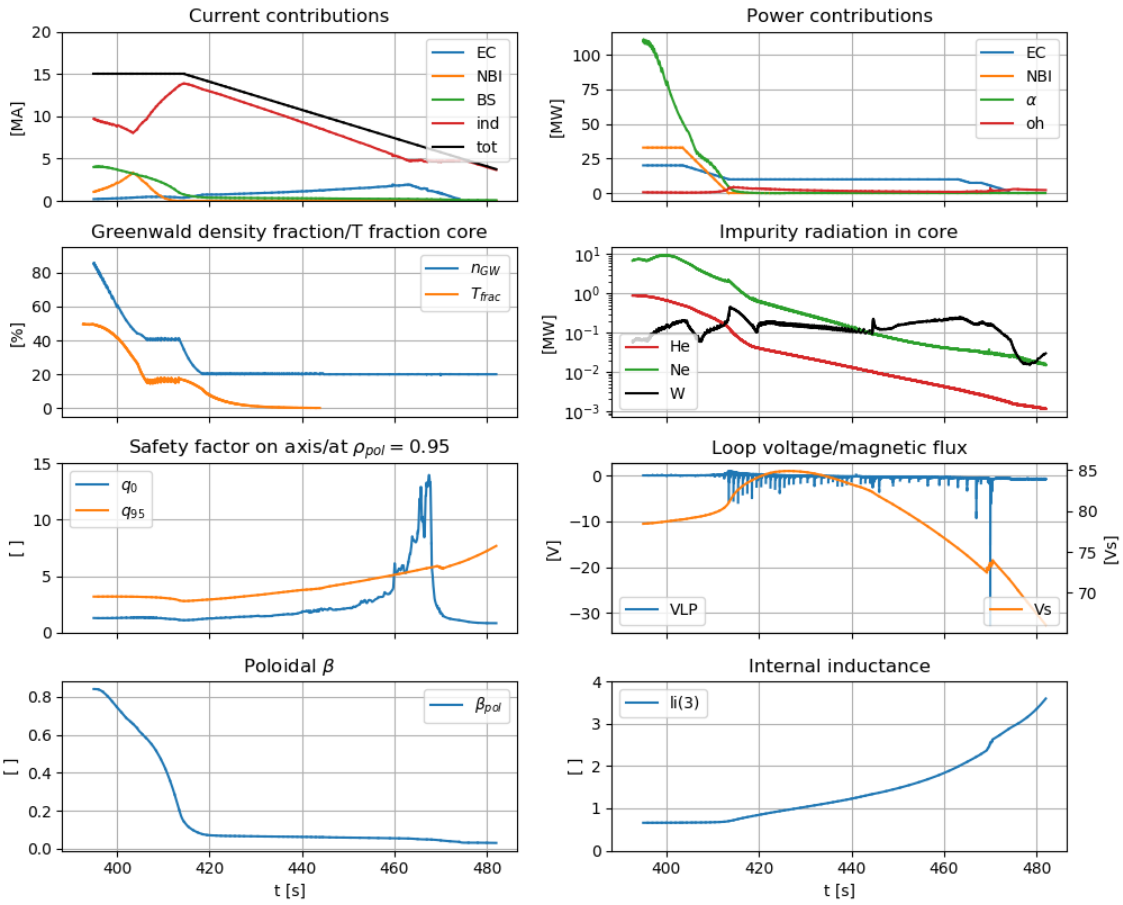

Figure 16. Time traces summarizing the exit phase starting from the flat-top burning phase at 395s.

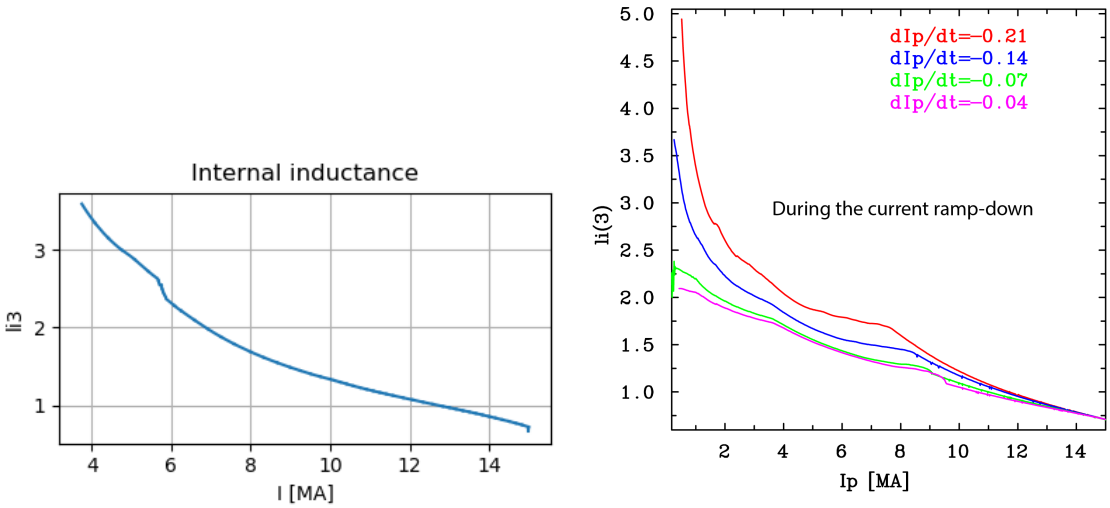

Figure 17. Internal inductance during the current ramp-down (left) compared to CORSICA simulations published in [29] taking into account vertical stability during the current-ramp-down. COMBINED IN ONE FIGURE?

rather quickly compared to what was previously expected. In these simulations the density is reduced from the flat-top value of 85% Greenwald density to 45% over 8s without lasting issues for heat load or radiation. The reduction of the pellet frequency during the density decay significantly reduces the fraction of tritium in the core though the fusion power and remaining auxiliary power in the power ramp down phase is enough to keep the plasma in H-mode. An H-L transition occurs at the end of the auxiliary power ramp down which is preferential for radial stability control. Finally, the total current is reduced from 15MA to 3.75MA in L-mode using a total current boundary condition.

Acknowledgement

JINTRAC was used under licence agreement between Euratom and CCFE, Ref. Ares(2014)3576010 -28/10/2014. This work was part funded by the RCUK Energy Programme [grant number EP/T012250/1], EPSRC Energy Programme [grant number EP/W006839/1]. and by ITER Task Agreement C19TD53FE implemented by Fusion for Energy under Grant GRT-869 and Contract OPE-1057. The views and opinions expressed herein do not necessarily reflect those of the ITER Organization. To obtain further information on the data and models underlying this paper please contact PublicationsManager@ukaea.uk.

References

[1] M. Romanelli *et al.*, Plasma fusion Res. 9 (2014) 3403023
[2] F. Koechl *et al.*, Nucl. Fusion **60**, 066015 (2020)
[3] E. Militello Asp *et al.*, Nucl. Fusion **62**, 126033 (2022)
[4] D. Farina *et al.*, Fusion Sci. Technol. **52**, 2 (2007) 154
[5] P. Strand, et al., Proc. 31st EPS Conference (London, UK, 2004)
[6] D. Harting *et al.*, 22^{nd} PSI Conference Rome, Italy (2016)
[7] G. Cenacchi and A. Taroni, Internal report, JET-IR(88)03
[8] R. Simonini *et al.*, Contrib. Plasma Phys. **34** 2-3 (1994) 368
[9] D. Reiter *et al.*, Fusion Sci. Technol. **47** 2 (2005) 172
[10] L. R. Baylor *et al.*, Nucl. Fusion **47**, 443-8 (2007)
[11] S. K. Combs *et al.* Fusion Eng. Des **75**, 691 (2005)
[12] B. Pégourié *et al.*, Nucl. Fusion **47** 1 (2007) 44
[13] A. R. Polevoi *et al.*, Nucl. Fusion **58** 056020 (2018)
[14] V. Kotov and D. Reiter, Plasma Physics Contr. Fusion **51** 115002 (2009)
[15] ITER Organisation Report no. ITR-18-003, internal report, ITER Organization, France, (2018)
[16] C. D. Challis *et al*, Nucl. Fusion **29** 563 (1989)
[17] F. Koechl *et al.*, Plasma Physics Contr. Fusion 074008 (2018)
[18] Y. R. Martin *et al.*, J. Phys. Conf. Ser **123**, 012003 (2008)
[19] Y. Gribov *et al.*, 43^{rd} EPS Conf. on Plasma Physics Leuven, Belgium (2016)
[20] V. Parail *et al.*, Nucl. Fusion **49** 7 (2009) 075030
[21] E. Militello Asp *et al.*, 29^{th} IAEA FEC London, UK (2023)
[22] W. A. Houlberg, Phys. Plasmas **4**, 3230 (1997)
[23] L. Garzotti *et al.*, Nucl. Fusion **59** (2019) 026006

[24] P. Belo *et al.* 42^{nd} EPS Conf. on Plasma Physics Lisbon, Portugal (2015)
[25] M. Fichtmueller *et al.*, Contrib. Plasma Phys. **38** 284 (1998)
[26] S. Maruyama *et al.*, 23^{rd} SOFE Conference 2009
[27] ITER Physics Expert Group on Confinement and Transport *et al.*, Nucl. Fusion **39** 12 (1999) 2175
[28] A. Portone *et al.*, Fusion Eng. Des. **74** 537 (2005)
[29] S. H. Kim *et al.*, Nucl. Fusion **58**, 056013 (2018)
[30] J. A. Crotinger *et al.*, 1997 LLNL Report UCRL-ID-126284; NTIS #PB2005-102154
[31] P. C. de Vries *et al.*, Nucl. Fusion **58**, 026019 (2018)